

THE PENNSYLVANIA STATE UNIVERSITY
SCHREYER HONORS COLLEGE

DEPARTMENT OF CHEMISTRY

Ice Nucleation of Functionalized Silver and Gold Nanoparticles and Zeolite Powders

DIVYA JAIN
FALL 2021

A thesis
submitted in partial fulfillment
of the requirements
for a baccalaureate degree
in Chemistry
with honors in Chemistry

Reviewed and approved* by the following:

Miriam A. Freedman
Professor of Chemistry
Thesis Supervisor

David Boehr
Associate Professor of Chemistry
Honors Advisor

Benjamin Lear
Associate Professor of Chemistry
Faculty Reader

* Electronic approvals are on file.

ABSTRACT

Heterogeneous ice nucleation is a field of atmospheric chemistry that has been studied for nearly 100 years on a variety of different particles. However, it has not focused on extensively isolating and varying surface groups that can act as a model system to isolate a specific functional group present on the surface of many atmospheric molecules. This study explores the effects of surface groups on the ice nucleation activity of silver nanoparticles, gold nanoparticles, and ZSM-5 zeolites via immersion freezing. Silver and gold nanoparticles are synthesized with analogous functional groups and the zeolites have varying ratios of Si/Al on the surface. All three particles are tested to assess which features lead to higher ice nucleation activity. Alcohol groups on the surface of the nanoparticle were found to be the most active, and higher alumina content on the surface of the zeolites correlated to higher activity. A better understanding of ice nucleation can lead to a deeper understanding of cloud formation, and by extension, climate.

TABLE OF CONTENTS

LIST OF FIGURES	iii
LIST OF TABLES	iv
ACKNOWLEDGEMENTS	v
Chapter 1 Introduction	1
Chapter 2 Materials and Methods	6
Silver Nanoparticles	6
Gold Nanoparticles	8
Zeolites	10
Experimental Set-Up	10
Data Analysis	11
Chapter 3 Results	13
Silver Nanoparticles	13
Gold Nanoparticles	17
Zeolites	20
Chapter 4 Discussion	23
Silver Nanoparticles	23
Gold Nanoparticles	25
Zeolites	27
Chapter 5 Conclusion	28
References	29

LIST OF FIGURES

Figure 1. Diagram of the Brust-Schiffrin Method for Synthesizing Silver Nanoparticles.....	7
Figure 2. Structures of functional groups.....	7
Figure 3. Diagram of the Brust-Schiffrin Method for Synthesizing Silver Nanoparticles.....	9
Figure 4. Immersion Freezing Chamber Set-Up.....	11
Figure 5. Aggregated Frozen Fraction Data for Silver Nanoparticles and structure of each of the ligands	14
Figure 6. Aggregated Normalized Freezing Data for Silver Nanoparticles.....	15
Figure 7. TEM image for functionalized silver nanoparticle. Top left: 1-undecanethiol AgNP (Scale: 20nm). Top Right: 4-mercaptobenzoic acid AgNP (Scale 200 nm). Bottom left: 11-mercapto-1-undecanoic AgNP (Scale 50 nm). Bottom Right: 11-mercapto-1-undecanol AgNP (Scale 200 nm).	16
Figure 8. Aggregated Frozen Fraction Data for Gold Nanoparticles.....	18
Figure 9. Aggregated Normalized Freezing Data for Gold Nanoparticles	19
Figure 10. TEM image for functionalized gold nanoparticle. Top left: 1-undecanethiol AuNP (Scale 50 nm). Top Right: 4-mercaptobenzoic acid AuNP (Scale 20 nm). Bottom left: 11-mercapto-1-undecanoic auNP (Scale 20 nm). Bottom Right: 11-mercapto-1-undecanol AuNP (Scale 20 nm).	20
Figure 11. Aggregated Frozen Fraction Data for Zeolite Powders. Note here that the molar ratio of $\text{SiO}_2/\text{Al}_2\text{O}_3$ for each zeolite varies according to the number. For example, P-38 should have a 38:1 molar ratio of $\text{SiO}_2/\text{Al}_2\text{O}_3$	21
Figure 12. Aggregated Normalized Freezing Data for Zeolite Powders. Note here that the molar ratio of $\text{SiO}_2/\text{Al}_2\text{O}_3$ for each zeolite varies according to the number. For example, P-38 should have a 38:1 molar ratio of $\text{SiO}_2/\text{Al}_2\text{O}_3$	22
Figure 13. Frozen Fraction of both silver and gold nanoparticles	25

LIST OF TABLES

Table 1. Tabulated Frozen Fraction Data for Silver Nanoparticles	13
Table 2. Tabulated Frozen Fraction Data for Gold Nanoparticles.....	17
Table 3. Tabulated Frozen Fraction Data for Zeolite Powders.....	20
Table 4. Results of XPS analysis on the ZSM-5 zeolite series. Note the infinite ratio of Si:Al for the P-38 zeolite.....	22

ACKNOWLEDGEMENTS

I would like to thank Dr. Miriam Freedman for guiding me through this project and for providing the materials and equipment necessary to complete it. I appreciate her for allowing me to undertake my own project as an undergraduate. I also want to thank Katie Marak and Esther Chong for being fantastic mentors throughout this project and continually helping me through each step of research. Especially with the unique challenges and struggles of the pandemic, your time and efforts are greatly appreciated! Additional thanks to Dr. David Boehr and Dr. Ben Lear for assistance during the thesis process and serving on my defense committee.

This material is based upon work supported by the National Science Foundation under Award No. NSF CHE-1904803. Any opinions, findings, and conclusions or recommendations expressed in this publication are those of the author(s) and do not necessarily reflect the views of the National Science Foundation.

Chapter 1

Introduction

Ice clouds, known as cirrus clouds, are formed from a collection of frozen water vapor particles, or ice crystals. In the atmosphere, water mostly freezes by a method called heterogeneous ice nucleation, wherein water vapor freezes on the surface of an aerosol particle, which serves as the nucleus for the ice crystal. Depending on where in the atmosphere the freezing occurs, there are four main mechanisms by which water vapor can freeze: immersion, deposition, contact, and condensation freezing.¹ This project focuses on immersion freezing, in which a water droplet surrounds a water insoluble particle. The interactions between the water and the surface of the particle lead to the formation of ice.²

At temperatures below 0 °C, water droplets do not freeze spontaneously; they can persist as supercooled liquids until they reach –38 °C, at which point they can freeze homogeneously without any nucleating particle. However, heterogeneous nucleation, water freezing on a particle surface, is far more common and occurs at warmer temperatures because it lowers the activation energy barrier to ice formation. Ice nuclei are generally insoluble particles, such as mineral dust or metallic material. Because of this, it is important to understand how the properties of atmospheric particles affect rates of nucleation.³

The atmosphere contains a wide variety of freely moving particles and gases. These particles are emitted from sources such as manufacturing/processing industries, vehicles, power plants, mineral dust from deserts, etc. In the atmosphere, these particles freely interact with each other and form complex products with many different physical and chemical properties. These

differing physical and chemical properties affect rates of ice nucleation significantly. Thus, it is essential to research these different physical and chemical properties that contribute to rates of ice nucleation. A better understanding of this can lead to a deeper understanding of cloud formation, and by extension, climate.⁴

During the past five decades, several different organic and inorganic materials have been studied as ice nucleation particles. For example, the ice nucleation activity of carbonaceous particles such as soot, one of the most commonly emitted pollutants, has been studied with differing chemical properties depending on its source.⁵ Groups have also studied fresh and aged mineral dusts, the most abundant ice nucleating particles, that originate from the Earth's crust.^{6,7} Bacteria have also been widely studied as ice nucleating particles, as they are able to freeze in relatively warmer temperatures at around -2 °C, and have found to be very good at ice nucleation.⁸ Oxidized organic aerosol particles are another group that have been recently studied as ice nucleating particles.⁹ Through these studies, it has been established that ice nucleating particles are prevalent in the atmosphere.

Previous experiments in the Freedman group have studied how to use engineered materials to finely tune surface properties to affect ice nucleation efficiency. Alstadt et al. have studied the effect of length and pore size of carbon nanotubes on its ice nucleation activity, finding that nanotubes less than 7nm and with inner diameters of 1–3 and 2–5 nm are most efficient.¹⁰ Various iron oxides have been studied to determine the effects of the role of lattice mismatch and defects induced by milling and hydroxyl exposure on ice nucleation activity.¹¹ A number of aluminum oxides and hydroxides have also been tested to study the effect of lattice match and crystallinity, finding that greater lattice match and crystallinity are most effective.¹²

Silver and gold nanoparticles are used for a wide range of purposes in research because they have unique chemical and physical properties when compared to compared to their solid bulk materials, stemming from their large surface area and electronic properties.¹³ However, this project takes a novel approach by using silver and gold nanoparticles for ice nucleation, which has not previously been done. Silver and gold nanoparticles are used in this project because they are simple systems that keep variables such as size, crystallinity, and porosity constant across the two systems and isolate the variable of functional groups and the crystal lattice structures.

Crystallinity of a particle has a contribution in how well ice nucleates. In general, greater crystallinity leads to higher ice nucleation activity.¹² In contrast, disorder at the surface leads to a decrease in activity. This is because ice stacks on the particle in a layer parallel to the surface. Therefore, an ordered plane would stabilize the basal plane of ice.¹⁵ Thus, the more amorphous and disordered the surface of the particle is, the more wrinkled the topography of the water and ice is, leading to smaller ordered domains and less freezing activity.¹⁵

Not only is the composition and crystallinity of the ice nucleus important, but also the surface characteristics. Important properties of surfaces include the ability of a surface to form hydrogen bonds promote water adsorption; the lattice structure of the ice nucleating particle should be similar to that of ice in order to better orient the water to form ice;¹² and heterogeneities such as pores and cavities on the surface of the particle should catalyze ice nucleation, as summarized by Pruppacher and Klett.¹⁶ In general, polar character and the ability of an ice nucleating particle to form hydrogen bonds to water greatly enhances freezing activity.

This study will explore what surface features promote ice nucleation. Using gold and silver nanoparticles will allow us to investigate how functional groups on the surface of nanoparticles affect ice nucleation of two crystalline materials with different lattice spacings.^{17 12}

Our hypothesis predicts that functional groups that are able to hydrogen bond with water and that the nanoparticles with crystalline lattice spacing closest to that of ice will have higher ice nucleation activity.

To test this, a set of functionalized silver and gold nanoparticles were synthesized via a modified Brust Schiffrin synthesis method¹⁸, characterized, and tested as ice nucleating particles in an immersion chamber. Each set of nanoparticles have an analogous set of functional groups attached to them which can be representative of the functional groups found in atmospheric particles formed as a result of atmospheric reactions, namely alcohols, carboxylic acids, and straight chain carbons. Thus, these experiments can determine which types of functional groups lead to higher ice nucleation activity than others. We predict that the alcohol functionalized nanoparticles will freeze best, followed by the carboxylic acid functionalized nanoparticles, and then the straight chain carbon functionalized nanoparticles.

Due to the coronavirus pandemic, research time was limited in the Spring 2020 and Fall 2020 semester. Therefore, in addition to the silver nanoparticle project, a set of ZSM-5 zeolite powders were also tested. Zeolites act as a model system for atmospheric mineral dust to understand the role of the surface porosity and composition in the nucleation process. Mineral dust is one of the most widely studied ice nucleating particles as it tends to travel far and wide in the atmosphere. For mineral dusts, the active sites are generally associated with defects like cracks and pores.¹⁹ In 1966, Fukuta already introduced that capillary condensation of water is essential for the ice nucleation ability of minerals.²⁰ In 2014, Marcolli introduced the importance of pore condensation and freezing.¹⁹ The surface of zeolites is highly microporous; this nature allows for greater capillary action and results in a surface that is potentially highly active for ice formation.

The zeolites used in this study have varying ratios of $\text{SiO}_2:\text{Al}_2\text{O}_3$, which we anticipate will affect the onset temperature of ice nucleation. Molar $\text{SiO}_2:\text{Al}_2\text{O}_3$ ratios have been controlled on ZSM-5 zeolites showing that the ratio affects the number of each functional group on the surface.²¹ Studies of water adsorption on the surface of zeolites have been studied thermodynamically in high silica, silico-alumina, and transition alumina microporous zeolites with pore sizes ranging from 0.5 to 0.75 nm.²² This study suggest that Al-containing sites have more affinity towards water than nanocavity confinement and therefore, greater ice nucleation activity. Therefore, we hypothesize that the zeolites with greater ratios of Al:Si will have greater ice nucleation activity.

Chapter 2

Materials and Methods

Silver Nanoparticles

The first step in conducting this project was finding a method of synthesizing the functionalized silver nanoparticles. The best method of synthesizing functionalized nanoparticles was determined to be the Brust-Schiffrin synthesis method¹⁸ due to ease of synthesis and functionalization ability. This method, shown in Figure 1, was discovered in 1994 and is known to create highly stable thiol-functionalized nanoparticles.²³ The general procedure for silver nanoparticle synthesis used in this project is found in literature and is described briefly here.²⁴

Materials used for the synthesis are as follows. Silver nitrate (>99.7%, JT Baker Chemical), sodium borohydride (>98%, Acris Organics), potassium nitrate (>99%, Sigma Aldrich), tetraoctylammonium bromide (TOAB, >98.0%, Sigma Aldrich), thiol ligands (11-mercapto-1-undecanol, 11-mercaptoundecanoic acid, 4-mercaptobenzoic acid, and 1-undecanethiol) (>96.0%, Sigma Aldrich), HPLC Grade water (Fischer Chemical), and absolute ethanol (200 proof, Fisher Chemical) were used without further purification.

AgNO_3 (169.88 mg, 1 mmol) in H_2O is combined with tetraoctylammonium bromide (1.6404 g, 3 mmol) in toluene and KBr (1.19 g, 10 mmol).²⁵ These are stirred vigorously for 30 min at 80°C. Then, the aqueous layer is removed and the organic layer is allowed to cool to room temperature. Then NaBH_4 (378.3 mg, 10 mmol), a reducing agent, in 0.4 °C H_2O is added to the reaction. Immediately after adding the reducing agent, the thiol ligand (1.5 mmol) in toluene is added. This reaction is allowed to run for 4 hours at room temperature. At completion, the organic layer is washed with H_2O three times and the organic solvent is removed via a stream of

nitrogen gas. Absolute ethanol is added to the dry mixture and it is sonicated for 15-20 min in order to create an evenly dispersed mixture. It is frozen overnight so that the silver nanoparticles crash out of solution and the byproducts and excess ligand remain suspended in solution. To remove the byproducts and excess ligands, the ethanol is decanted. The remaining precipitate is washed with 0.4 °C absolute ethanol via centrifugation at 10,000 rpm for 10 minutes five times.

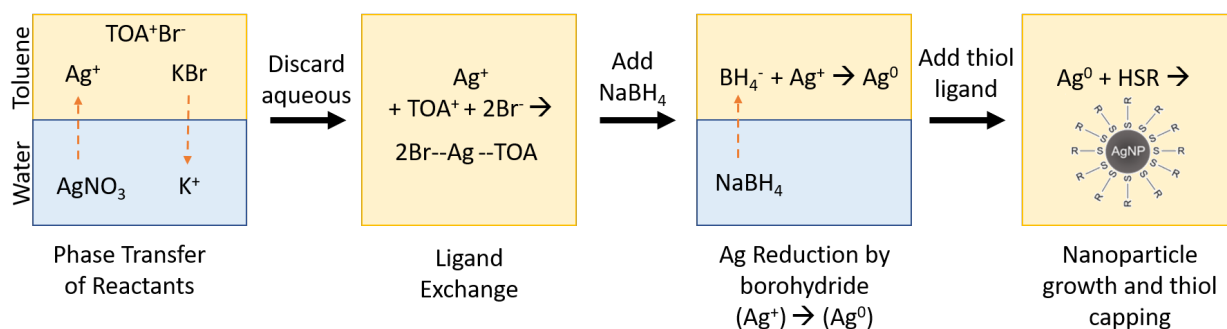


Figure 1. Diagram of the Brust-Schiffrin Method for Synthesizing Silver Nanoparticles

Using this synthesis method, a set of four thiol functionalized silver nanoparticles were produced using the ligands 1-undecanethiol, as the straight carbon chain, 4-mercapto benzoic acid, 11-mercapto-1-undecanol, and 11-mercaptoundecanoic acid, shown in Figure 2. Medium length aliphatic chain functional group ligands were chosen because they were more likely to form ordered domains on the surface of the molecule.^{26 27}

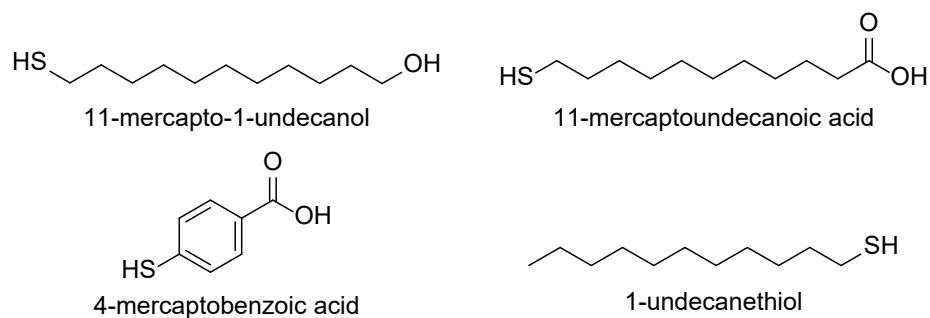


Figure 2. Structures of functional groups

Gold Nanoparticles

An analogous set of gold nanoparticles was synthesized by Santana Cruz in Lear lab using the Brust Schiffrin method, as illustrated in Figure 3¹⁸ and the Turkevich method.²⁸ This set was produced using the same ligands as the silver nanoparticles. Nanopure water was used at 18.2 $M\Omega \cdot \text{cm}^{-1}$ purity. Tetraoctylammonium bromide (TOAB, >98.0%, TCI), 1-undecanethiol (>96.0%, TCI), sodium borohydride (99%, VenPure SF powder, Acros Organics), sodium hydroxide (98.5%, for analysis pellets, Acros Organics) gold (III) chloride hydrate (99.995%, Sigma Aldrich), tannic acid (Sigma Aldrich), and 4-mercaptobenzoic acid (99%, Sigma Aldrich), potassium carbonate (99.0% min, Alfa Aesar), Sodium citrate tribasic dihydrate (Fluka Analytical), 1-mercaptoundecanoic acid (Chem Cruz), toluene (Fischer Chemical), and methanol (Fischer Chemical) were used without further purification.

Gold undecanethiol-protected nanoparticles were synthesized via a modified Brust-Schiffrin method. $\text{HAuCl}_4 \cdot \text{x H}_2\text{O}$ (302 mg, 0.889 mmol) was dissolved in 25 mL of nanopure water. TOAB (2.1989 g, 4.02 mmol) was dissolved in 60mL of toluene by stirring for 5 min. The aqueous AuCl_4^- solution was added to the TOAB solution, and the two-phase mixture was vigorously stirred for 10 min. The aqueous layer was removed and 1-undecanethiol (630 μL , 2.813mmol) was added to the stirring organic phase. Immediately following the addition of the ligand, a freshly prepared aqueous solution of 0.4 °C NaBH_4 (0.3825g, 25mL) was added dropwise to the solution and the reaction was allowed to stir for 3 hours. To purify the particles, the precipitate was collected via centrifugation at 10,000rpm for 7 min, resulting in a particle pellet in a clear and colorless supernatant. The supernatant was decanted off into the waste and the particles were redispersed in ca. 2-3 mL of toluene and ca. 37-38 mL of methanol and the

centrifugation process was repeated once more. Dried AuNPs with a typical yield of 200 mg were collected.

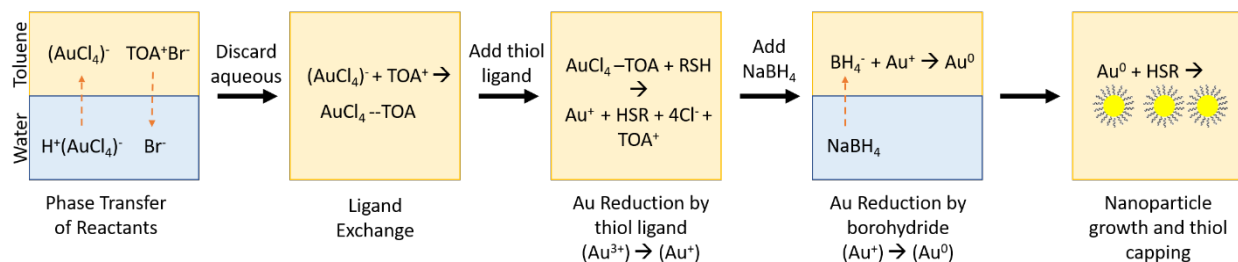


Figure 3. Diagram of the Brust-Schiffrin Method for Synthesizing Silver Nanoparticles

Gold 4-mercaptopbenzoic acid and 11-mercaptopundecanoic acid protected nanoparticles were synthesized via a reported modified Turkevich method, while 11-mercaptop-1-undecanol particles were synthesized via a modified Turkevich method.²⁸ Sodium citrate tribasic dihydrate (0.0970 g, 0.333 mmol) was dissolved in 150mL of nanopure water by vigorously stirring to produce a clear and colorless solution. Tannic acid (2.5mM, 0.1mL) was added into the solution, followed by potassium carbonate (150mM, 1mL) to adjust the pH of the solution to 11. The clear and colorless solution was heated to 68 - 69 °C in an oil bath. Once the solution reached 68 - 69 °C, $HAuCl_4$ (28mM, 1mL) was added to the stirring reaction. The solution was allowed to stir for an additional 15 minutes at 68 - 69°C to ensure the complete reduction of gold. The citrate-protected AuNPs were used as the parent particles for the protected AuNPs.

To synthesize the gold 4-mercaptopbenzoic acid and the 11-mercaptopundecanoic acid protected nanoparticles, a stock solution of 1mM of each thiol ligand was made by dissolving 0.0026g 4-mercaptopbenzoic acid or 0.0035g 11-mercaptopundecanoic acid, respectively, into 15mL of nanopure water alongside 1 pellet of NaOH. Then, the 200μL of the ligand solution was added to the 20mL of citrate-protected AuNPs. The particles were allowed to stir overnight

at room temperature. The particles were filtered and concentrated using a 30,000 kDA molecular weight cutoff filter (Amicon Ultra - 4). The particles were centrifuged at 10,000rpm for 2 minutes to filter and concentration from 5mL to 500 μ L. This was repeated until all 20mL of the particles were concentrated to 2mL. Finally, the particles were washed with nanopure water and suspended in hexanes.

To synthesize the gold 11-mercapto-1-undecanol nanoparticles, A stock solution of 1mM 11-mercapto-1-undecanol was made by dissolving 0.0038g 11-mercapto-1-undecanol into 15mL of ethanol. Then, the 200 μ L of the ligand solution was added to the 20mL of citrate-protected AuNPs and allowed to stir for 1 hour. The particles were centrifuged at 10,000 rpm for 7 minutes. The supernatant was decanted off and the pellet was readily dispersed in ethanol.

Zeolites

The zeolites used were ZSM-5 zeolite powders purchased from ACS Materials. A set of four zeolites were used: MR-25, P-38, P-117, and P-360, with reported molar ratios of 25:1, 38:1, 117:1, and 360:1 SiO₂: Al₂O₃, respectively.

Experimental Set-Up

The immersion freezing chamber has been discussed in detail by Alstadt et al.²⁶ and is described here briefly. The chamber is a low moisture environment used to test ice nucleation of the droplets. The chamber is an enclosed system with two purified nitrogen streams that flow into it. One stream is a purge flow that prevents condensation inside the chamber. The other stream of nitrogen is cooled by liquid nitrogen and then passed through the immersion chamber

to cool it at a rate of $-3\text{ }^{\circ}\text{C}/\text{min} \pm 0.3\text{ }^{\circ}\text{C}/\text{min}$. $2\text{ }\mu\text{L}$ droplets ($\sim 0.7\text{ }\mu\text{m}$ diameter) of $0.02\text{ wt } \%$ solution in ultrapure water (Millipore Q, $18.2\text{ }\Omega\cdot\text{cm}^2$) are pipetted onto silanized slides (Hampton Research). A temperature probe attached to the copper plate near the slide and monitors the internal temperature of the chamber. A camera situated above the chamber takes photos of the droplets every $-0.5\text{ }^{\circ}\text{C}$ from $0\text{ }^{\circ}\text{C}$ to $-30\text{ }^{\circ}\text{C}$ or until all the droplets freeze. At least 2 trials of 122 droplets are performed for each particle.

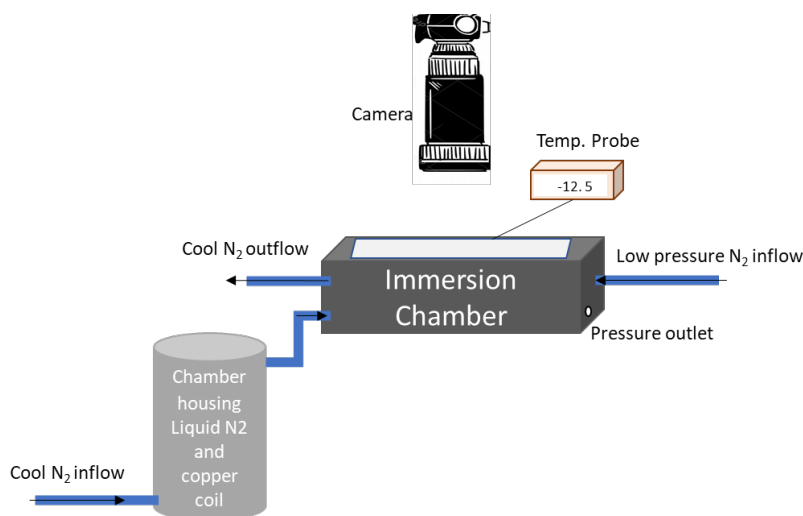


Figure 4. Immersion Freezing Chamber Set-Up.

The immersion chamber houses a slide with the droplets being tested in a trial. A stream of N_2 gas is cooled and enters the chamber to cool it, with a temperature probe monitoring the temperature drop. A low-pressure flow of N_2 gas flows through the chamber to remove ambient water vapor to prevent it from interfering with the freezing of the droplets.

Data Analysis

We display our results in terms of both frozen fraction and normalized based on the surface area of the particles. Results of the immersion trials are first given in the form of frozen fraction data, detailing what fraction of droplets freeze at which temperatures. Frozen Fraction is given by

$$F(T) = \frac{n(T)}{N}$$

where $n(T)$ is the total number of frozen droplets at a given temperature and N is the total number of droplets in the sample population.¹²

In order to normalize the freezing to surface area and to account for homogeneous freezing of water and normalize freezing based on per unit surface area of the particles, further calculations were carried out based on Vali et al. and O'Sullivan et al.^{27,28} In these, $K(T)$, the number of nucleation sites per milliliter of water at a specific temperature is determined for each trial. The equation for $K(T)$ is given by:

$$K(T) = \frac{-\ln [1 - F(T)]}{V}$$

where $F(T)$ is the fraction of droplets frozen at a specific temperature, V is the drop volume in milliliters. The $K(T)$ value for nanopure water was subtracted from the $K(T)$ value of each particle data set to account for background freezing.

The cumulative number of active surface sites per cm^2 as a function of temperature (n_s) was calculated from $K(T)$ using the equation:

$$n_s = K(T) \times C^{-1}$$

where C is the total surface area in a given volume. C was calculated from the BET surface area for silver nanoparticles and TEM for the gold nanoparticles, and the weight percent of the silver nanoparticle and zeolite samples prepared for immersion freezing, and from TEM for the gold nanoparticles.^{27,28} Active surface sites are the sites on the surface of a particle where ice nucleation occurs. For each average $K(T)$, n_s was calculated using the standard deviation of the $K(T)$ of each trial. This produces a graph where the freezing of the particle is normalized per cm^2 , with an example shown in Figure 6.

Chapter 3

Results

Silver Nanoparticles

Table 1 indicates that the particles froze in a span of 10-12 degrees with 1-undecanethiol freezing in the shortest span of 9.5 degrees, followed by 4-mercaptobenzoic acid with 10 degrees, then 11-mercaptoundecanoic with 11.5 degrees, and lastly 11-mercapto-1-undecanol in a 12 degrees range. The onset temperature of the silver nanoparticles followed the order of 11-mercapto-1-undecanol AgNP, then 4-mercaptobenzoic acid AgNP and 11-mercaptoundecanoic acid at the same temperature, followed by 1-undecanethiol. In terms of 50% freezing, 11-mercapto-1-undecanol froze at the warmest temperatures, then 4-mercaptobenzoic acid, and lastly 1-undecanethiol and 11-mercaptoundecanoic at the same temperature.

Table 1. Tabulated Frozen Fraction Data for Silver Nanoparticles

(in °C)	1-undecanethiol	4-mercaptobenzoic acid	11-mercapto-1-undecanol	11-mercaptoundecanoic acid
Freezing Onset	-14.5	-12	-8.5	-12
50% Frozen	-20.5	Between -17.5 & -18	Between -16.5 to -17	-20.5
100% Frozen	-24	-22	-20.5	-23.5

Figure 5 shows this tabulated data in figure form, showing the frozen fraction freezing data. From the frozen fraction data, we see that 11-mercapto-1-undecanol freezes at the warmer temperatures, followed by 4-mercaptobenzoic acid, then 11-mercaptoundecanoic acid and 1-undecanethiol.

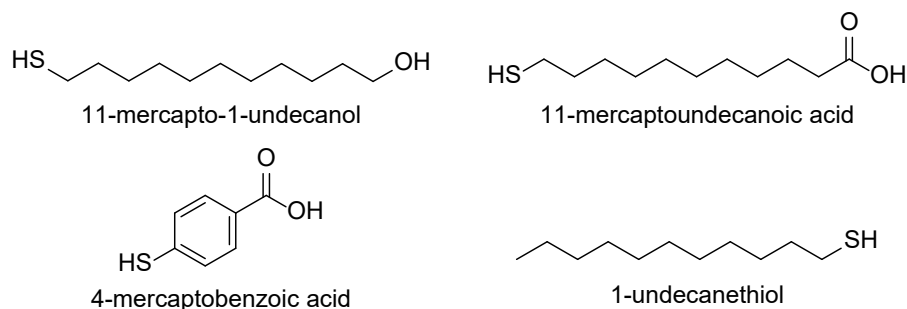
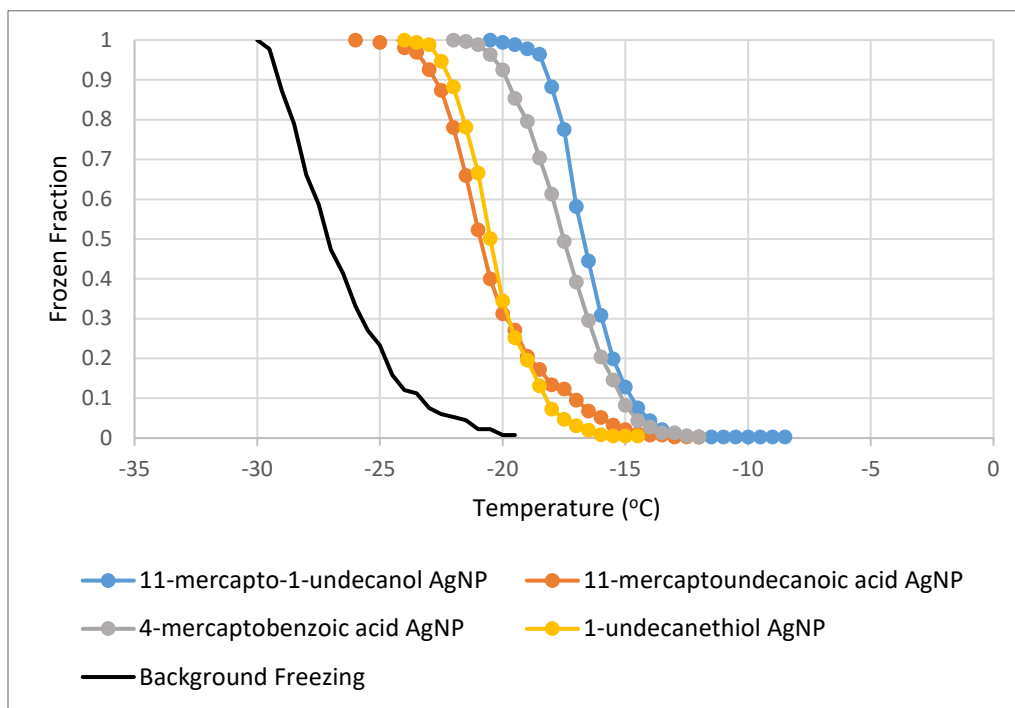


Figure 5. Aggregated Frozen Fraction Data for Silver Nanoparticles and structure of each of the ligands

The surface area of a gram of particles was calculated based on BET analysis in order to normalize the frozen fraction to the number of active sites per gram of particle. Figure 6 shows the graph of the silver nanoparticles freezing normalized to the surface area of the particles. The general freezing trend remains the same as with the frozen fraction data. 1-undecanol AgNP is the best ice nucleating particle, followed by 4-mercaptobenzoic acid AgNP. 11-mercaptoundecanoic AgNP and 1-undecanethiol AgNP have similar rates of freezing. This

correlates with the number of active sites on the surface of the particle. 1-undecanol AgNP had the greatest active sites of all the silver nanoparticles with 162 active sites per cm^2 at -18°C .

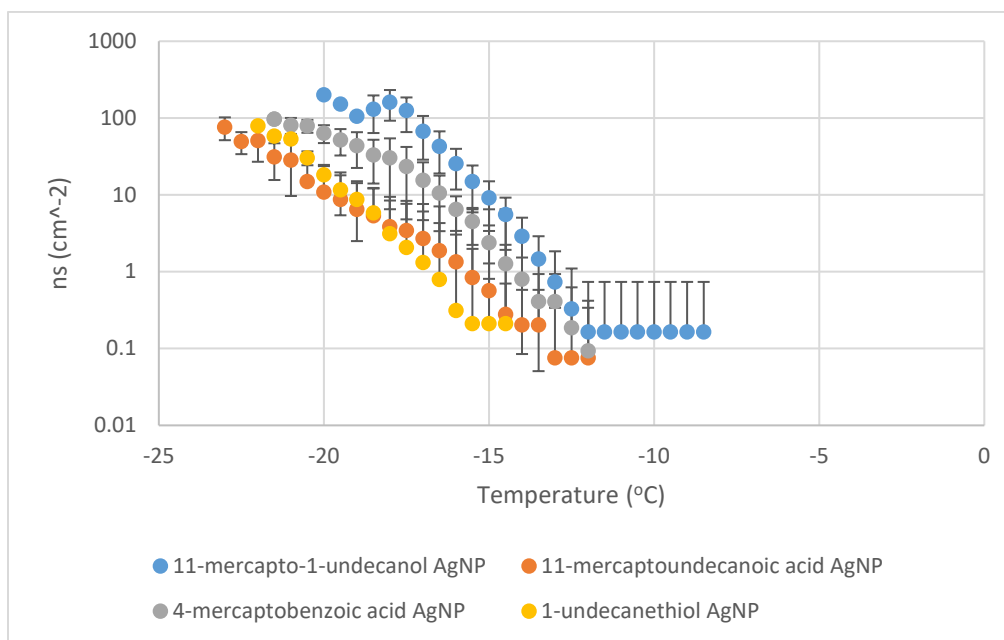


Figure 6. Aggregated Normalized Freezing Data for Silver Nanoparticles.

Error bars on the data points in the graph represent the error between the eight different trials that test about 244 droplets

In Figure 6, several data points end some degrees earlier than the frozen fraction data points. This is due to the calculation of $K(T)$ to determine n_s . Within the four tests that were conducted for each trial, if one of the tests ended earlier than another, then some of the data points are undefined by the equation for $K(T)$. Thus, the average $K(T)$ can only be calculated to the warmest temperature at which all of the droplets are frozen.

Some of the negative side of the error bars are also not given for data points. This is because the error extended below zero, which cannot be graphed on a logarithmic plot. In addition, n_s does not increase proportionally with decreasing temperature for all of the samples because the removal of background freezing can cause fluctuations in the graph.¹²

TEM data was collected on each of the four functionalized silver nanoparticles, shown in Figure 7. It is clear that the nanoparticles formed aggregates, most likely due to the drop-cast

method that the TEM grids were prepared with. However, we do see that the nanoparticles have a round shape, meeting the desired expectations from the synthesis. The approximate diameters as seen in the TEM images are as follows: 1-undecanethiol – 4nm, 4-mercaptobenzoic acid – 33nm, 11-mercaptoundecanoic – 2.5nm, 11-mercapto-1-undecanol – 18 nm.

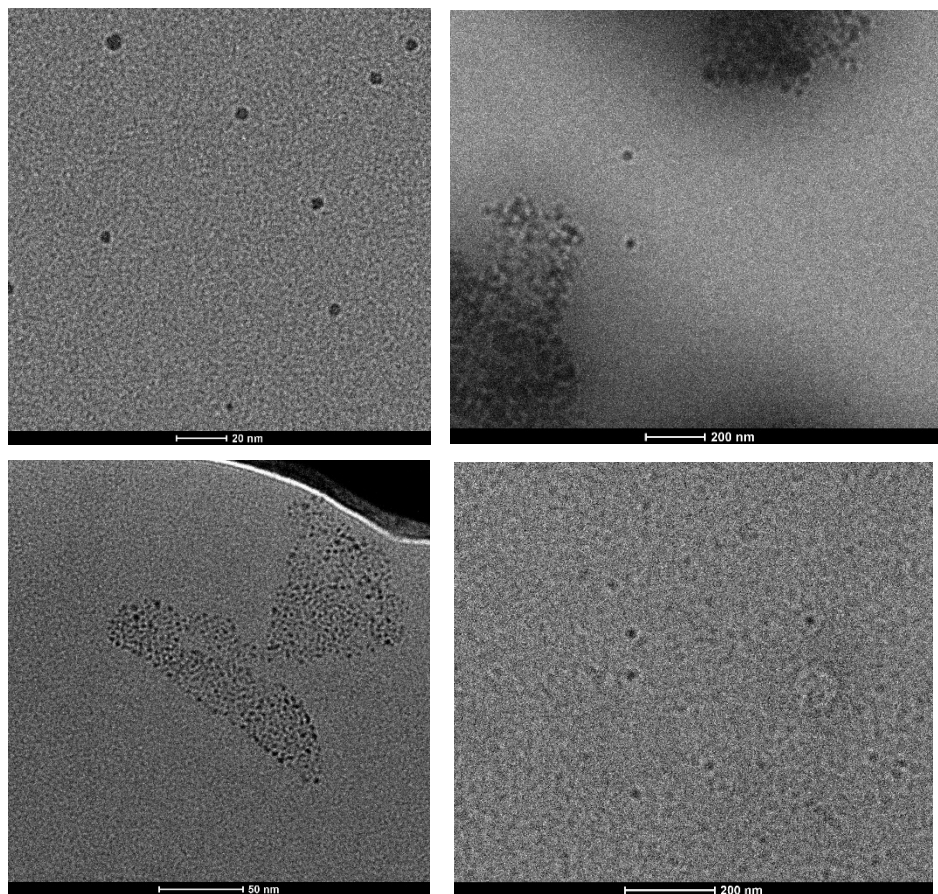


Figure 7. TEM image for functionalized silver nanoparticle. Top left: 1-undecanethiol AgNP (Scale: 20nm). Top Right: 4-mercaptobenzoic acid AgNP (Scale 200 nm). Bottom left: 11-mercapto-1-undecanoic AgNP (Scale 50 nm). Bottom Right: 11-mercapto-1-undecanol AgNP (Scale 200 nm).

Gold Nanoparticles

Table 2 indicates that the particles froze in a span of 7-12 degrees with 4-mercaptobenzoic acid freezing in the shortest span of 7 degrees, followed by 11-mercapto-1-undecanol with a 11 degree range, then 11-mercaptoundecanoic in 11.5 degrees, and lastly 1-undecanethiol in a 12 degree range. The freezing onset order was first 11-mercapto-1-undecanol, then 11-mercaptoundecanoic, followed by 4-mercaptobenzoic acid, and lastly 1-undecanethiol. In terms of 50% freezing, 11-mercapto-1-undecanol froze at the highest temperatures, then 4-mercaptobenzoic acid and 11-mercaptoundecanoic, and lastly 1-undecanethiol.

Table 2. Tabulated Frozen Fraction Data for Gold Nanoparticles

(in °C)	1-undecanethiol	4-mercaptobenzoic acid	11-mercapto-1-undecanol	11-mercaptoundecanoic acid
Freezing Onset	-17.5	-17	-8.5	-14.5
50% Frozen	-22	-21.5	-11 to -11.5	-21.5
100% Frozen	-29.5	-24	-19.5	-26

Figure 8 shows this tabulated data in figure form, showing the frozen fraction freezing data. From the frozen fraction data, we see that 11-mercapto-1-undecanol freezes at the warmer temperatures, followed by 4-mercaptobenzoic acid and 11-mercaptoundecanoic acid, and lastly 1-undecanethiol.

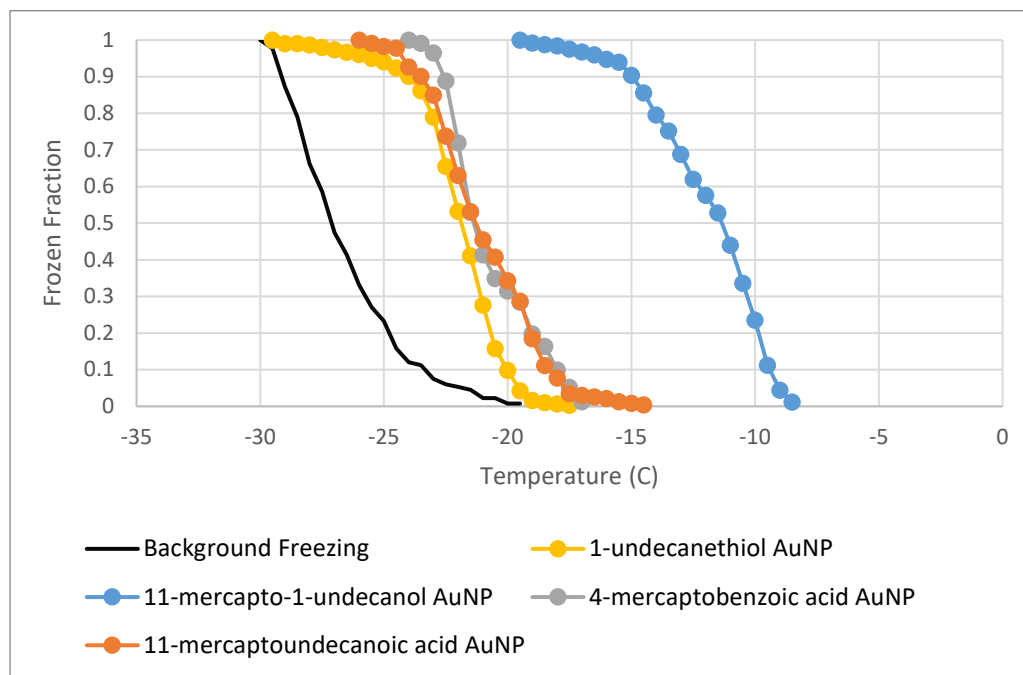


Figure 8. Aggregated Frozen Fraction Data for Gold Nanoparticles

The surface area of a gram of particles was calculated based on TEM analysis in order to normalize the frozen fraction to the number of active sites per cm^2 per gram of particle. Figure 9 shows the graph of the gold nanoparticles freezing normalized to the surface area of the particles. The general freezing trend remains the same as with the frozen fraction data. 1-undecanol AuNP is the best ice nucleating particle, followed by 1-undecanoic AuNP and 4-mercaptopbenzoic acid AuNP, and lastly, 1-undecanethiol AuNP. It is supported by the n_s value of 14 active sites per cm^2 at $-15\text{ }^\circ\text{C}$, the greatest of all the gold nanoparticles. This order is similar to that of the silver nanoparticles. However, it is important to note that because the surface area was calculated by TEM rather than by BET, as it was with the silver nanoparticles, the results are not directly comparable because there could be greater estimation errors with the gold nanoparticles surface areas.

In Figure 9, as with the silver nanoparticles, several data points end some degrees earlier than the frozen fraction data points and some of the negative sides of the error bars are also not given for data points due to the same reasons outlined previously.

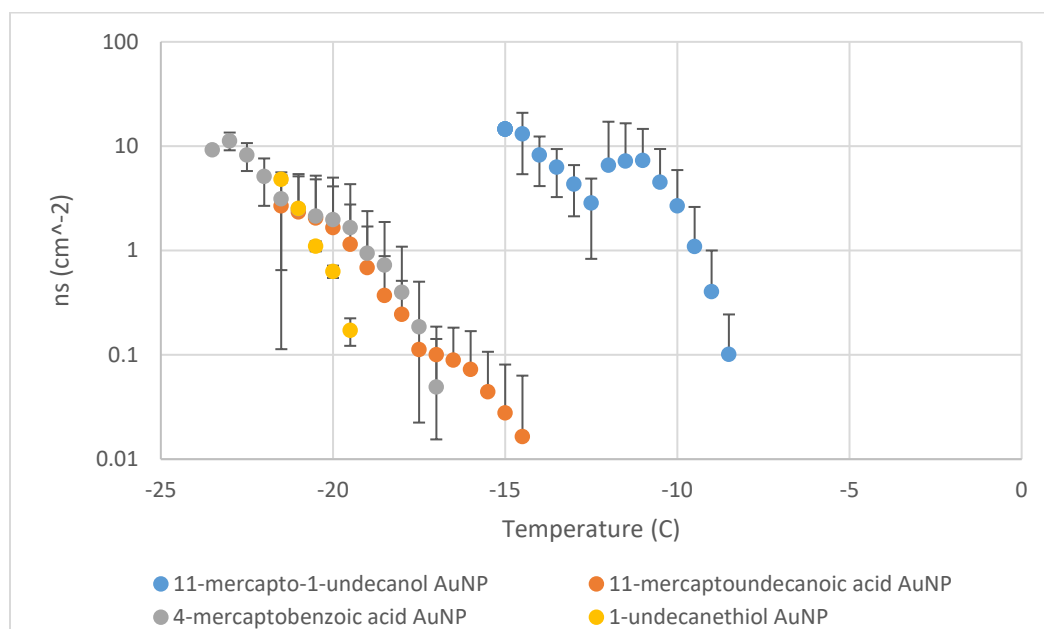


Figure 9. Aggregated Normalized Freezing Data for Gold Nanoparticles
Error bars on the data points in the graph represent the error between the eight different trials that test about 244 droplets

TEM data was collected on each of the four functionalized silver nanoparticles, shown in Figure 10. As with silver, the nanoparticles have a round shape, meeting the desired expectations from the synthesis. The approximate diameters as seen in the TEM images are as follows: 1-undecanethiol – 3.6 ± 0.5 nm, 4-mercaptobenzoic acid – 2.5 ± 0.4 nm, 11-mercaptopundecanoic – 2.0 ± 0.3 nm, 11-mercapto-1-undecnaol – 4.6 ± 1.0 nm.

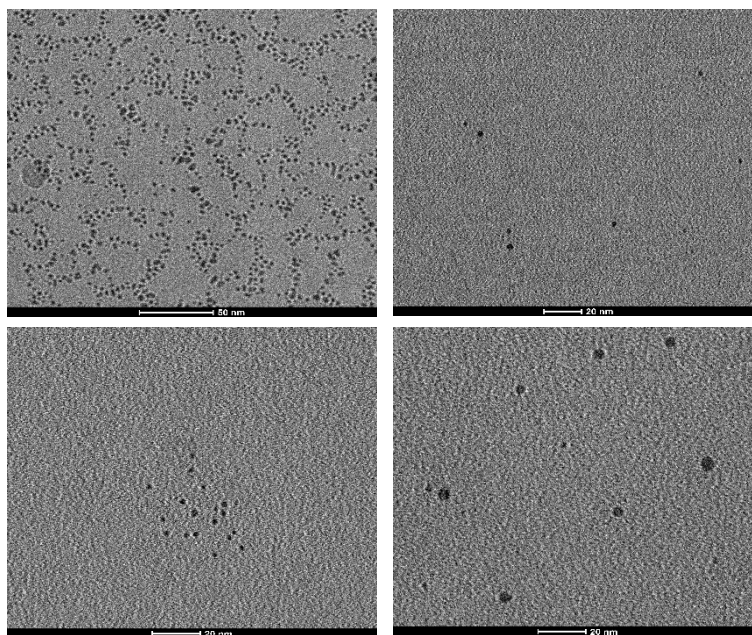


Figure 10. TEM image for functionalized gold nanoparticle. Top left: 1-undecanethiol AuNP (Scale 50 nm). Top Right: 4-mercaptopbenzoic acid AuNP (Scale 20 nm). Bottom left: 11-mercaptop-1-undecanoic auNP (Scale 20 nm). Bottom Right: 11-mercaptop-1-undecanol AuNP (Scale 20 nm).

Zeolites

Table 3 shows that the zeolites froze in a span of 6.5-13 degrees with P-117 freezing in the shortest span of 6.5 degrees, followed by MR-25 in 7.5 degrees, then P-360 in 12 degrees, and lastly P-38 in a 13 degree range. The freezing onset order of the molecules is P-117, followed by MR-25, then P-360, and lastly P-38. In terms of 50% freezing, P-117 froze at the warmest temperatures, then MR-25 closely after, followed by P-360, and lastly P-38.

Table 3. Tabulated Frozen Fraction Data for Zeolite Powders

(in °C)	MR-25	P-38	P-117	P-360
Freezing Onset	-10	-15	-9	-13
50% Frozen	Between -12.5 to -13	Between -24.5 to -25	-12.5	-19
100% Frozen	-17.5	-28	-15.5	-25

Figure 11 shows this tabulated data in figure form, showing the frozen fraction freezing data. From the frozen fraction data, we see that P-117 and MR-25 freeze at warmer temperatures, followed by P-360 and then P-38. Interestingly, we see that P-117 has the most active sites of the set of zeolites, with 3 per cm^2 at -17°C .

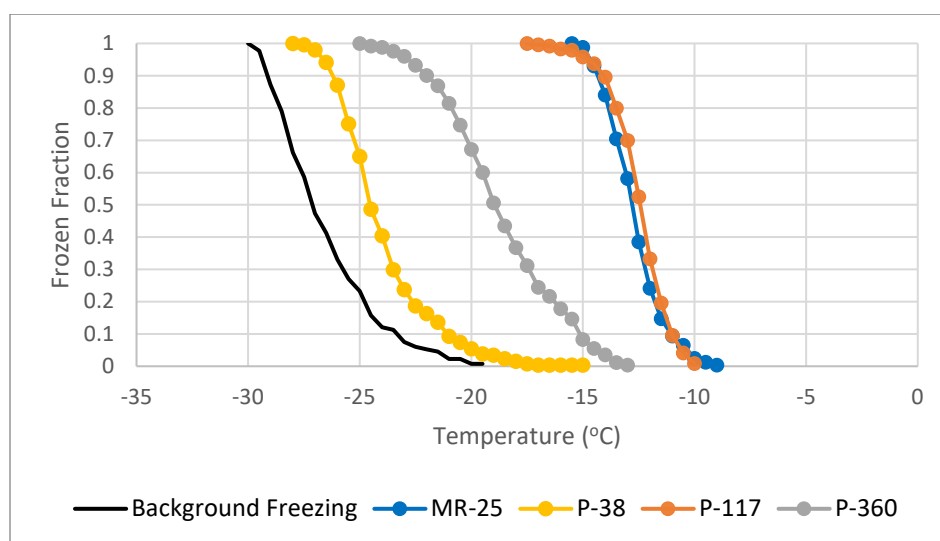


Figure 11. Aggregated Frozen Fraction Data for Zeolite Powders. Note here that the molar ratio of $\text{SiO}_2/\text{Al}_2\text{O}_3$ for each zeolite varies according to the number. For example, P-38 should have a 38:1 molar ratio of $\text{SiO}_2/\text{Al}_2\text{O}_3$

As with the silver nanoparticles, the surface area of a gram of the zeolite powders was found through BET analysis in order to normalize the frozen fraction to the number of active sites per gram of particle. The freezing, normalized to surface area, is shown in Figure 12. Again, note that some negative error bars are not shown for the reasons outlined before for silver nanoparticles. The normalized general freezing trend follows the frozen fraction data. MR-25 and P-117 are the best ice nucleating particles, followed by P-360 and then P-38.

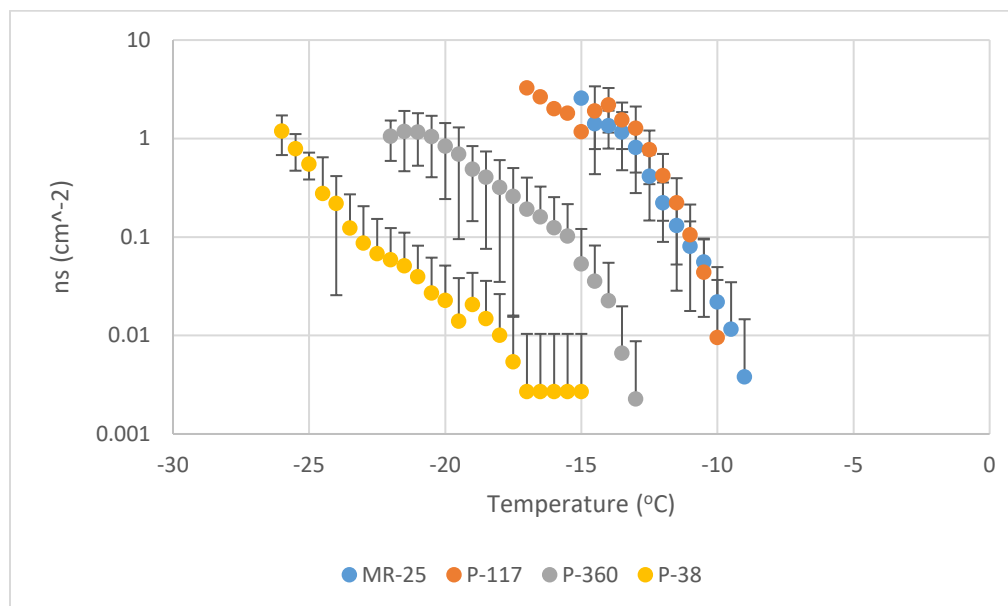


Figure 12. Aggregated Normalized Freezing Data for Zeolite Powders. Note here that the molar ratio of $\text{SiO}_2/\text{Al}_2\text{O}_3$ for each zeolite varies according to the number. For example, P-38 should have a 38:1 molar ratio of $\text{SiO}_2/\text{Al}_2\text{O}_3$. Error bars on the data points in the graph represent the error between the eight different trials that test about 244 droplets

XPS data was collected on the zeolites to confirm the reported surface properties from the manufacturer, as shown in Table 4. The table indicates that the reported ratios of Si:Al from the manufacturer were not consistent with the results from the XPS analysis. While the ratios should have been MR-25, P-38, P-117, and P-360, with molar ratios of 25:1, 38:1, 117:1, and 360:1 $\text{SiO}_2: \text{Al}_2\text{O}_3$, respectively, the XPS shows that MR-25 actually had a ratio of 20:1, P-38 was essentially all Si, P-117 was 28:1, and P-360 was 513:1.

Table 4. Results of XPS analysis on the ZSM-5 zeolite series. Note the undefined ratio of Si:Al for the P-38 zeolite

Sample	C^{total}	Al	Si	Si:Al
MR-25	4.4	1.4	29.2	20
P-38	2.0	-	31.0	undefined
P-117	5.4	1.1	30.1	28
P-360	12.1	0.1	28.5	513

Chapter 4

Discussion

Silver Nanoparticles

Ice nucleation is affected by the surface of the material that ice is nucleating on. Literature indicates that different functional groups contribute to ice nucleation differently. Hydrophilic functional groups tend to nucleate ice at warmer temperatures than hydrophobic groups due to increased favorable interactions with water.³¹ Therefore, a larger concentration of hydroxyl groups on the surface will lead to freezing at warmer temperatures.³² Cox et al. have found that groups that promote the right equilibrium of hydrogen bonding in which the water is adsorbed to the ligand, creating order of the water, but is not bound so tightly that it prevents water-water interactions, have the highest ice nucleation activity.³³ Carboxylic acids are very polar and hydrogen bond more strongly than hydroxyl groups, and therefore have lower ice nucleation activity. These studies help to explain the freezing trends from the silver nanoparticles of 1-undecanol AgNP being most active, followed by 4-mercaptobenzoic acid AgNP, then 11-mercaptoundecanoic acid, and lastly 1-undecanethiol.

1-undecanol AgNP has the highest activity because it is an alcohol functional group on the surface of the particle that can interact with water via hydrogen bonding. Parungo suggests that alcohol groups are the most effective, followed by halogens, carboxylic acids, and esters within substituted benzoic acid groups.³⁴ Hydrogen bonding adsorbs water onto the surface of the particle and create ordering, facilitating ice formation.³³

Both of the carboxylic acid functional groups (4-mercaptobenzoic acid and 1-undecanoic acid) have different rates of freezing. 4-mercaptobenzoic acid AgNP is a more active ice

nucleating particle because the benzene ring in the body of the ligand provides rigidity so that the carboxylic acids are more ordered on the surface of the silver nanoparticle, increasing the number of active sites available for freezing.¹⁵ Further, the 4-mercaptobenzoic acid AgNP was much larger (~33 nm) as compared to the 1-undecanoic AgNP (~2.5 nm). As suggested by Kanji and Abbatt, particles of greater surface area lead to great ice nucleation activity due to the availability of more active sites in a more favorable surface structure.³⁵ Prauchpper and Klett have generally found that ice nucleating particles should be 100 nm or more in size to be effective.¹⁶ However, we can see here that these smaller particles can be effective too, and this which has been found by the Molinero group as well.¹⁵

1-undecanoic AgNP simply has a long carbon chain which may cause disordered stacking of the ligand chains of the carboxylic acids, which is less conducive to ice nucleation, as found by Qiu et al.¹⁵. Lastly, 1-undecanethiol is worst at freezing due to its hydrophobic nature; there is no hydrophilic functional group to improve freezing rates or form hydrogen bonds with the surrounding water.

Gold Nanoparticles

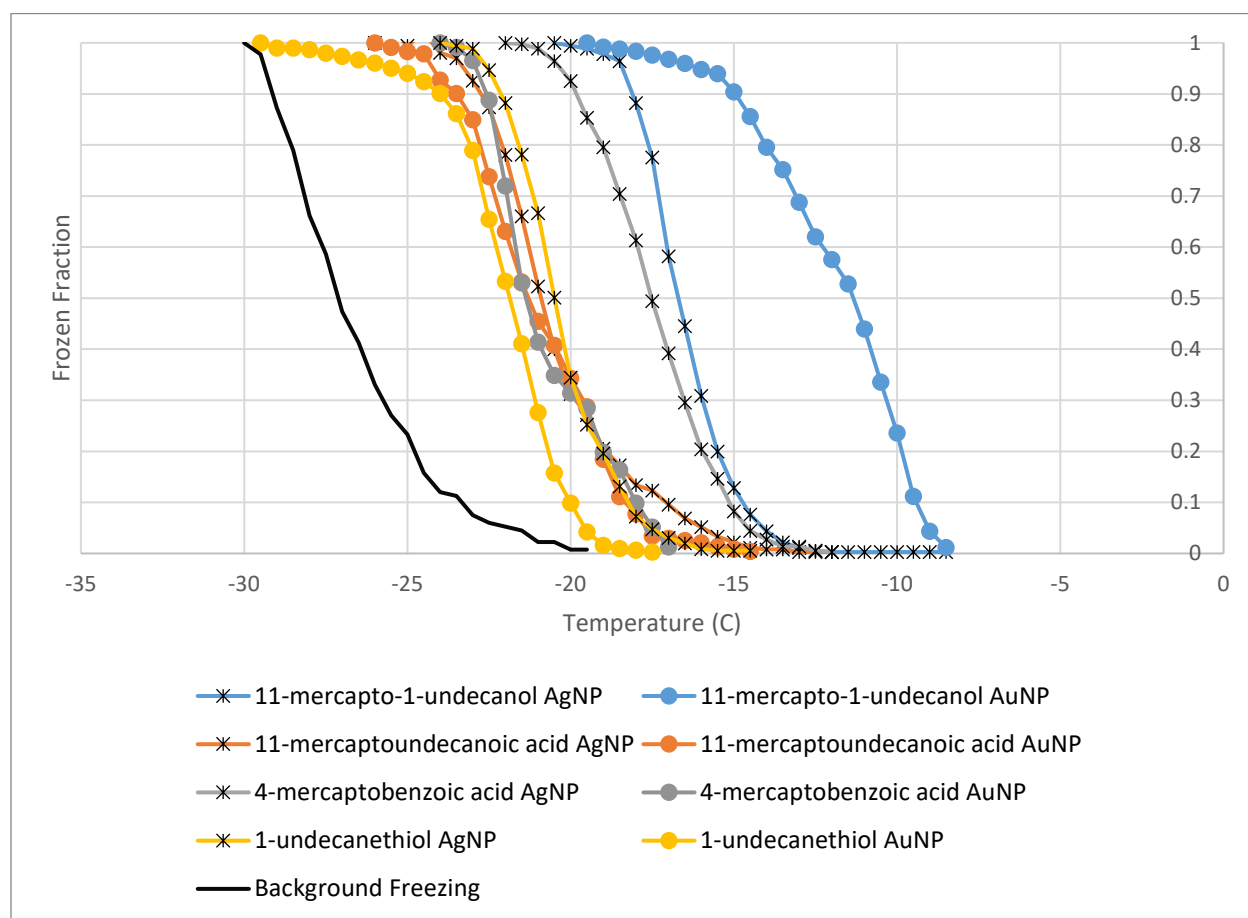


Figure 13. Frozen Fraction of both silver and gold nanoparticles

The order of freezing for the gold nanoparticles nearly matched the order of freezing for the silver nanoparticles: the alcohol NP being the best, followed by the carboxylic acid NPs, and then the straight chain carbon NP. However, in the gold, the 11-mercaptoundecanoic acid nanoparticles freeze essentially at the same time as 4-mercaptobenzoic nanoparticles. This is different than the silver nanoparticles, which show a more distinct ordering of freezing, likely based on the floppiness of the ligands, but this rigidity effect is not observed with the carboxylic acid gold nanoparticles.

11-mercapto-1-undecanol NPs froze in essentially the same range for both silver and gold nanoparticles. The silver nanoparticles froze in $-8.5\text{ }^{\circ}\text{C}$ to $-20.5\text{ }^{\circ}\text{C}$ with 50% frozen at $16.5\text{ }^{\circ}\text{C}$. Gold nanoparticles froze in $-8.5\text{ }^{\circ}\text{C}$ to $-19.5\text{ }^{\circ}\text{C}$ but the 50% frozen fraction was at $-11\text{ }^{\circ}\text{C}$, about 5.5 degrees earlier than in silver. 1-undecanethiol NPs froze at warmer temperatures on silver nanoparticles than gold nanoparticles. For the silver, the freezing began 3 degrees warmer and ended 5.5 degrees warmer than gold; the 50% frozen mark was 1.5 degrees sooner as well. In terms of the freezing range, it froze in a smaller span of ten degrees in silver versus twelve degrees for gold. 4-mercaptobenzoic acid froze at warmer temperatures for silver, but froze in a larger range of 10 degrees for silver versus 7 degrees as gold. The silver nanoparticles started freezing 5 degrees warmer and ended freezing two degrees warmer. 11-mercaptoundecanoic acid begins freezing at two degrees warmer for silver than gold and ends freezing at 2.5 degrees warmer.

Overall, it seems that the silver nanoparticles functionalized at warmer temperatures than the gold nanoparticles, with the exception of the 11-mercapto-1-undecanol NP. To investigate the reasons as to why, the lattice spacing of silver and gold were compared to that of ice, with the hypothesis that silver nanoparticles froze faster because the lattice spacing of it is closer to that of ice. The (111) hexagonal lattice spacing for silver is 2.32 \AA ,³⁶ for gold is 2.36 \AA ,³⁷ and for ice is 2.75 \AA .¹² This indicates that the lattice spacing difference of the silver and gold is so small that it does not significantly affect the spacings of the ligands. Therefore, lattice spacings would not have a significant effect on its ice nucleation activity. Thus, more research will be needed to determine the reasons as to why silver nanoparticles freeze faster than gold nanoparticles.

Zeolites

The hypothesis for the freezing trend is that the zeolites with the highest ratio of alumina would serve as the best ice nucleating particle, as aluminum shows higher ice nucleation than silica due to a greater hydrogen bonding between hydroxyl groups on the surface with water and closer crystal structure matching with ice.^{2,12} However, although framework aluminum is important, water can adsorb even without the presence of aluminum, which indicates that it adsorbs at defect sites, impurities, and the Si-O-Si framework.^{22,38,39} It is important to note that water absorption is weaker on the surface silanol groups than the rapid adsorption on aluminum frameworks.³⁸ For this reason, water should still freeze on the high percentage silica particles at warmer temperatures than the background freezing.

Based on these studies, the freezing, in order of best particle to worst should have been MR-25>P-38>P-117>P-360. MR-25 followed this trend, but the trend observed for the other particles was P117>P-360>P-38. This was an unexpected result, so the zeolites, especially the P-38 zeolite, should be characterized further in order to investigate why it was not as good of an ice nucleating particle.

XPS was performed on the zeolite powders in order to see what surface groups containing silica and aluminum are present, as well as their potential to form hydrogen bonds with water. Table 4 shows the results of the XPS testing, and helps to clarify the unexpected trend in ice nucleation activity. Although the P-38 should have had aluminum on the surface, the XPS analysis shows that there is none actually present. Therefore, the data fits our original hypothesis that zeolites with higher ratios of alumina have higher ice nucleation activity.

Chapter 5

Conclusion

This study explored the ice nucleating activity of three different particles: silver nanoparticles, gold nanoparticles, and zeolites, in order to determine the effect of the surface characteristics in immersion freezing experiments. A set of analogous functional silver and gold nanoparticles were synthesized and characterized and a set of zeolites with varying ratios of $\text{Al}_2\text{O}_3:\text{SiO}_2$ were purchased. All particles underwent ice nucleation tests in an immersion chamber to test ice nucleation activity, which was normalized to the particle's surface area.

We found that ice nucleation activity depended on the groups on the surface of the particles. The general freezing trends for nanoparticles found that the alcohol functionalized nanoparticles froze best, followed by the two carboxylic acid nanoparticles, and then lastly the straight-chain carbon functionalized nanoparticles. Silver nanoparticles were found to freeze at warmer temperatures than gold nanoparticles, and further investigation is needed to look into the causes. Additionally, we found that the carboxylic acid AgNPs has a distinct freezing order with the less floppy ligand, 4-mercaptobenzoic acid functionalized NPs, freezing at warmer temperatures than 11-mercaptoundecanoic acid AgNPs. For zeolites, those with higher ratios of $\text{Al}_2\text{O}_3:\text{SiO}_2$ showed freezing at warmer temperatures.

The experimental data confirmed the hypothesis that ligands that can hydrogen bond with water strongly enough to promote adsorption and create ordering of the water, but not too strongly to prevent water-water interactions and subsequent ice growth have the highest ice

nucleation activity. Additionally, surface groups that match the crystalline structure of ice more closely, namely alumina, promote higher ice nucleation activity.

This study adds to literature on how crystallinity and functional groups impact ice nucleation. This body of research is critical to understanding how ice nucleation processes happen in the atmosphere, and ultimately, affect climate.

References

- (1) Vali, G. Nucleation Terminology. *J. Aerosol Sci.* **1985**, *16*, 575–576.
- (2) Freedman, M. A. Potential Sites for Ice Nucleation on Aluminosilicate Clay Minerals and Related Materials. *Journal of Physical Chemistry Letters* **2015**, *6* (19), 3850–3858.
<https://doi.org/10.1021/acs.jpcclett.5b01326>.
- (3) Hoose, C.; Lohmann, U.; Erdin, R.; Tegen, I. The Global Influence of Dust Mineralogical Composition on Heterogeneous Ice Nucleation in Mixed-Phase Clouds. *Environ. Res. Lett* **2003**, *3* (2).
- (4) Adams, P.; Donahue, N.; Pandis, S. Atmospheric Particles and Climate Change. *AIChE Journal* **2013**, *59* (11), 4006–4019. <https://doi.org/10.1002/aic>.
- (5) Mahrt, F.; Marcolli, C.; David, R.; Gronquist, P.; Barthazy Meier, E.; Lohmann, U.; Kanji, Z. Ice Nucleation Abilities of Soot Particles Determined with the Horizontal Ice Nucleation Chamber. *Atmos. Chem. Phys.* **2018**, *18* (18), 13362–13392.
- (6) Zolles, T.; Burkart, J.; Häusler, T.; Pummer, B.; Hitzenberger, R.; Grothe, H. Identification of Ice Nucleation Active Sites on Feldspar Dust Particles. *Journal of Physical Chemistry A* **2015**, *119* (11), 2692–2700. <https://doi.org/10.1021/jp509839x>.
- (7) Salam, A.; Lesins, G.; Lohmann, U. Laboratory Study of Heterogeneous Ice Nucleation in Deposition Mode of Montmorillonite Mineral Dust Particles Aged with Ammonia, Sulfur Dioxide,

- and Ozone at Polluted Atmospheric Concentrations. *Air Quality, Atmosphere and Health* **2008**, *1* (3), 135–142. <https://doi.org/10.1007/s11869-008-0019-6>.
- (8) Mortazavi, R.; Hayes, C. T.; Ariya, P. A. Ice Nucleation Activity of Bacteria Isolated from Snow Compared with Organic and Inorganic Substrates. *Environmental Chemistry* **2008**, *5* (6), 373–381. <https://doi.org/10.1071/EN08055>.
- (9) Li, J.; Forrester, S. M.; Knopf, D. A. Heterogeneous Oxidation of Amorphous Organic Aerosol Surrogates by O₃, NO₃, and OH at Typical Tropospheric Temperatures. *Atmospheric Chemistry and Physics* **2020**, *20* (10), 6055–6080. <https://doi.org/10.5194/acp-20-6055-2020>.
- (10) Alstadt, V. J.; Dawson, J. N.; Losey, D. J.; Sihvonen, S. K.; Freedman, M. A. Heterogeneous Freezing of Carbon Nanotubes: A Model System for Pore Condensation and Freezing in the Atmosphere. *Journal of Physical Chemistry A* **2017**, *121* (42), 8166–8175. <https://doi.org/10.1021/acs.jpca.7b06359>.
- (11) Chong, E.; Marak, K. E.; Li, Y.; Freedman, M. A. Ice Nucleation Activity of Iron Oxides via Immersion Freezing and an Examination of the High Ice Nucleation Activity of FeO. *Physical Chemistry Chemical Physics* **2021**, *23* (5), 3565–3573. <https://doi.org/10.1039/d0cp04220j>.
- (12) Chong, E.; King, M.; Marak, K. E.; Freedman, M. A. The Effect of Crystallinity and Crystal Structure on the Immersion Freezing of Alumina. *Journal of Physical Chemistry A* **2019**, *123* (12), 2447–2456. <https://doi.org/10.1021/acs.jpca.8b12258>.
- (13) Alaqad, K.; Saleh, T. A. Gold and Silver Nanoparticles: Synthesis Methods, Characterization Routes and Applications towards Drugs. *Journal of Environmental & Analytical Toxicology* **2016**, *6* (4). <https://doi.org/10.4172/2161-0525.1000384>.
- (14) Slepíčka, P.; Kasálková, N. S.; Siegel, J.; Kolská, Z.; Švorčík, V. Methods of Gold and Silver Nanoparticles Preparation. *Materials* **2020**, *13* (1), 1. <https://doi.org/10.3390/ma13010001>.
- (15) Qiu, Y.; Odendahl, N.; Hudait, A.; Mason, R.; Bertram, A. K.; Paesani, F.; DeMott, P. J.; Molinero, V. Ice Nucleation Efficiency of Hydroxylated Organic Surfaces Is Controlled by Their

- Structural Fluctuations and Mismatch to Ice. *Journal of the American Chemical Society* **2017**, *139* (8), 3052–3064. <https://doi.org/10.1021/jacs.6b12210>.
- (16) Pruppacher, H. R.; Klett, J. D. *Microphysics of Clouds and Precipitation*; Luwer Academic Publishers: Boston, MA, 1997.
- (17) Ganguly, M.; Dib, S.; Ariya, P. A. Purely Inorganic Highly Efficient Ice Nucleating Particle. *ACS Omega* **2018**, *3* (3), 3384–3395. <https://doi.org/10.1021/acsomega.7b01830>.
- (18) Brust, M.; Walker, M.; Bethell, D.; Schiffrin, D. J.; Whyman, R. Synthesis of Thiol-Derivatised Gold Nanoparticles in a Two-Phase Liquid-Liquid System. *J. Chem. Soc., Chem. Commun.* **1994**, 801–802.
- (19) Marcolli, C. Deposition Nucleation Viewed as Homogeneous or Immersion Freezing in Pores and Cavities. *Atmospheric Chemistry and Physics* **2014**, *14* (4), 2071–2104. <https://doi.org/10.5194/acp-14-2071-2014>.
- (20) Fukuta, N. Activation of Atmospheric Particles as Ice Nuclei in Cold and Dry Air. *Journal of Atmospheric Sciences* **1966**, 741–750.
- (21) Hernández, M. A.; Abbaspourrad, A.; Petranovskii, V.; Rojas, F.; Portillo, R.; Salgado, M. A.; Hernández, G.; Velazco, M. de los A.; Ayala, E.; Quiroz, K. F. Estimation of Nanoporosity of ZSM-5 Zeolites as Hierarchical Materials. *Zeolites and Their Applications* **2018**, No. September 2020. <https://doi.org/10.5772/intechopen.73624>.
- (22) Bolis, V.; Busco, C.; Ugliengo, P. Thermodynamic Study of Water Adsorption in High-Silica Zeolites. *Journal of Physical Chemistry B* **2006**, *110* (30), 14849–14859. <https://doi.org/10.1021/jp061078q>.
- (23) Perala, S. R. K.; Kumar, S. On the Mechanism of Metal Nanoparticle Synthesis in the Brust-Schiffrin Method. *Langmuir* **2013**, *29* (31), 9863–9873. <https://doi.org/10.1021/la401604q>.
- (24) Battocchio, A.; Meneghini, C.; Fratoddi, I.; Vendetti, I.; Russo, M.; Aquilanti, A.; Maurizio, C.; Bondino, F.; Matassa, R.; Rossi, M.; Mobilo, A.; Polzonetti, G. Silver Nanoparticles Stabilized

- with Thiols: A Close Look at the Local Chemistry and Chemical Structure. *J. Phys. Chem. C* **2012**, *116* (36), 19571–19578.
- (25) Booth, S. G.; Uehara, A.; Chang, S. Y.; la Fontaine, C.; Fujii, T.; Okamoto, Y.; Imai, T.; Schroeder, S. L. M.; Dryfe, R. A. W. The Significance of Bromide in the Brust-Schiffrin Synthesis of Thiol Protected Gold Nanoparticles. *Chemical Science* **2017**, *8* (12), 7954–7962. <https://doi.org/10.1039/c7sc03266h>.
- (26) Gavish, M.; Popovitz-Biro, R.; Lahav, M.; Leiserowitz, L. Ice Nucleation by Alcohols Arranged in Monolayers at the Surface of Water Drops. *Science* **1990**, *250*, 973–975.
- (27) Bolintineanu, D. S.; Lane, J. M. D.; Grest, G. S. Effects of Functional Groups and Ionization on the Structure of Alkanethiol-Coated Gold Nanoparticles. *Langmuir* **2014**, *30* (37), 11075–11085. <https://doi.org/10.1021/la502795z>.
- (28) Hoque, M. M.; Mayer, K. M.; Ponce, A.; Alvarez, M. M.; Whetten, R. L. Toward Smaller Aqueous-Phase Plasmonic Gold Nanoparticles: High-Stability Thiolate-Protected 4.5 Nm Cores. *Langmuir* **2019**, *35* (32), 10610–10617. <https://doi.org/10.1021/acs.langmuir.9b01908>.
- (29) O'Sullivan, D.; Murray, B. J.; Ross, J. F.; Whale, T. F.; Price, H. C.; Atkinson, J. D.; Umo, N. S.; Webb, M. E. The Relevance of Nanoscale Biological Fragments for Ice Nucleation in Clouds. *Scientific Reports* **2015**, *5*, 1–7. <https://doi.org/10.1038/srep08082>.
- (30) Gabor, V. Quantitative Evaluation of Experimental Results on the Heterogeneous Freezing Nucleation of Supercooled Liquids. *Journal of the Atmospheric Sciences* **1971**, *28*, 402–409.
- (31) Coluzza, I.; Creamean, J.; Rossi, M. J.; Wex, H.; Alpert, P. A.; Bianco, V.; Boose, Y.; Dellago, C.; Felgitsch, L.; Fröhlich-Nowoisky, J.; Herrmann, H.; Jungblut, S.; Kanji, Z. A.; Menzl, G.; Moffett, B.; Moritz, C.; Mutzel, A.; Pöschl, U.; Schauer, M.; Scheel, J.; Stopelli, E.; Stratmann, F.; Grothe, H.; Schmale, D. G. Perspectives on the Future of Ice Nucleation Research: Research Needs and Unanswered Questions Identified from Two International Workshops. *Atmosphere* **2017**, *8* (8). <https://doi.org/10.3390/atmos8080138>.

- (32) Xue, H.; Lu, Y.; Geng, H.; Dong, B.; Wu, S.; Fan, Q.; Zhang, Z.; Li, X.; Zhou, X.; Wang, J. Hydroxyl Groups on the Graphene Surfaces Facilitate Ice Nucleation. *Journal of Physical Chemistry Letters* **2019**, *10* (10), 2458–2462. <https://doi.org/10.1021/acs.jpcelett.9b01033>.
- (33) Cox, S. J.; Kathmann, S. M.; Slater, B.; Michaelides, A. Molecular Simulations of Heterogeneous Ice Nucleation. I. Controlling Ice Nucleation through Surface Hydrophilicity. *Journal of Chemical Physics* **2015**, *142* (18). <https://doi.org/10.1063/1.4919714>.
- (34) Parungo, F.; Lodge Jr., J. Molecular Structure and Ice Nucleation of Some Organics. *J. Atmos. Sci.* **1965**, *22*, 309–313.
- (35) Kanji, Z. A.; Abbatt, J. P. D. Ice Nucleation onto Arizona Test Dust at Cirrus Temperatures: Effect of Temperature and Aerosol Size on Onset Relative Humidity. *Journal of Physical Chemistry A* **2010**, *114* (2), 935–941. <https://doi.org/10.1021/jp908661m>.
- (36) Khan, M. A. M.; Kumar, S.; Ahamed, M.; Alrokayan, S. A.; AlSalhi, M. S. Structural and Thermal Studies of Silver Nanoparticles and Electrical Transport Study of Their Thin Films. *Nanoscale Research Letters* **2011**, *6* (1), 1–8. <https://doi.org/10.1186/1556-276X-6-434>.
- (37) Wang, Y. Q.; Liang, W. S.; Geng, C. Y. Coalescence Behavior of Gold Nanoparticles. *Nanoscale Research Letters* **2009**, *4* (7), 684–688. <https://doi.org/10.1007/s11671-009-9298-6>.
- (38) Olson, D. H.; Haag, W. O.; Borghard, W. S. Use of Water as a Probe of Zeolitic Properties: Interaction of Water with HZSM-5. *Microporous and Mesoporous Materials* **2000**, *35–36*, 435–446. [https://doi.org/10.1016/S1387-1811\(99\)00240-1](https://doi.org/10.1016/S1387-1811(99)00240-1).
- (39) Ng, E. P.; Mintova, S. Nanoporous Materials with Enhanced Hydrophilicity and High Water Sorption Capacity. *Microporous and Mesoporous Materials* **2008**, *114* (1–3), 1–26. <https://doi.org/10.1016/j.micromeso.2007.12.022>.

ACADEMIC VITA

DIVYA JAIN

EDUCATION

**The Pennsylvania State University
Schreyer Honors College**

Eberly College of Science B.S. in Chemistry

Environmental Engineering Minor, Smeal Business Fundamentals Certificate

Dean's List: 7/7 semesters

University Park, PA

Graduation: Dec 2021

RELEVANT COURSE WORK

International Business Operations, Environmental Chemistry, Chemistry of Fuels, Water Quality Chemistry, Intro to Management & Organization, Principles of Energy Engineering, Wastewater Treatment, Supply Chain Management, Intro to Environmental Engineering, Foundations of Sustainable Leadership, Technical Writing, Intro to Finance, Leadership Jumpstart, Intro to Financial & Managerial Accounting

Fall 2017-Fall 2021

PROFESSIONAL EXPERIENCE

Supply Chain Consulting Intern, EY, Atlanta Office

Virtual

- Created a dashboard in Power BI to visualize historical inventory data by compiling, analyzing, and presenting multiple data sets in a user-intuitive format
- Supported team by creating software training documents for client, creating and delivering project status updates to client, and summarizing data for client presentations

June-August 2021

Drawdown Research Scholar, Penn State College of Engineering

Virtual

- Analyzed framework and data of PSU Dining along with integrating information from several members of Dining staff to strategize how to reduce its carbon footprint
- Recommended tangible steps to improve sustainability based on life cycle analyses

June-August 2020

Chemical Engineering Co-op at Anheuser-Busch

Houston, TX

- Worked in the Utilities department as a manager and engineer
- Carried out inter-departmental projects to help reduce natural resource use, specifically managing influent to wastewater treatment facility and boosting operator performance
- Learned skills in excel and data analysis to improve key performance indicators

Jan. 2019 - July 2019

CO-CURRICULARS

Student Representative on Presidential Carbon Emissions Reductions Task Force

University Park, PA

- Appointed by the President of PSU to serve on a Task Force to research solutions on how to reduce university carbon emissions and set a new university-wide carbon neutrality goal

May-August 2021

Member of Student Sustainability Advisory Council

University Park, PA

- Student liaison to executive administration, crafting and presenting long-term sustainability strategies for the university, appointed by PSU President

Fall 2018 - Present

Executive Co-Director of Penn State Climate Action

University Park, PA

- Collaborating with student and staff to collect over 2,000 signatures of support to create institutional changes for Penn State to combat climate change and lead in sustainability

March 2020-Present

Eco-Action Club President and Earth Day Director

University Park, PA

- Educating members and the greater Penn State community on how to be an environmentally-engaged citizen and campaigning to make Penn State a more sustainable institution

Aug. 2018 - Dec. 2020

AWARDS

John Roe Sustainability Impact Award

University Park, PA

- Presented by the Penn State Sustainability Institute to recognize students who cultivate opportunities to advance the Sustainable Development Goals while demonstrating personal integrity, fostering justice, and strengthening partnerships.

April 2021

American Chemical Society Division of Environmental Chemistry Undergraduate Student Award

University Park, PA

- Presented by the Penn State Chemistry Department

May 2021